Journal of Biomolecular NMR, 10 (1997) 63–75

J-Bio NMR 448

^{1}H, ^{15}N and ^{13}C NMR resonance assignment, secondary structure and global fold of the FMN-binding domain of human cytochrome P450 reductase

Igor Barsukov[a], Sandeep Modi[a,b], Lu-Yun Lian[a], Kong Hung Sze[a], Mark J.I. Paine[c], C. Roland Wolf[c] and Gordon C.K. Roberts[a,b,*]

[a]*Department of Biochemistry and Biological NMR Centre and* [b]*Centre for Mechanisms of Human Toxicity, University of Leicester, Leicester LE1 9HN, U.K.*
[c]*Biomedical Research Centre, Ninewells Hospital and Medical School, University of Dundee, Dundee DD1 9SY, U.K.*

Received 3 January 1997
Accepted 24 March 1997

Keywords: Cytochrome P450 reductase; Flavin mononucleotide; Triple resonance; Resonance assignment; Semiautomatic

Summary

The FMN-binding domain of human NADPH-cytochrome P450 reductase, corresponding to exons 3–7, has been expressed at high level in an active form and labelled with ^{13}C and ^{15}N. Most of the backbone and aliphatic side-chain ^{1}H, ^{15}N and ^{13}C resonances have been assigned using heteronuclear double- and triple-resonance methods, together with a semiautomatic assignment strategy. The secondary structure as estimated from the chemical shift index and NOE connectivities consists of six α-helices and five β-strands. The global fold was deduced from the long-range NOEs unambiguously assigned in a 4D ^{13}C-resolved HMQC-NOESY-HMQC spectrum. The fold is of the alternating α/β type, with the five β-strands arranged into a parallel β-sheet. The secondary structure and global fold are very similar to those of the bacterial flavodoxins, but the FMN-binding domain has an extra short helix in place of a loop, and an extra helix at the N-terminus (leading to the membrane anchor domain in the intact P450 reductase). The experimental constraints were combined with homology modelling to obtain a structure of the FMN-binding domain satisfying the observed NOE constraints. Chemical shift comparisons showed that the effects of FMN binding and of FMN reduction are largely localised at the binding site.

Introduction

NADPH-cytochrome P450 oxidoreductase (P450 reductase) is an essential component of the cytochrome P450 monooxygenase system found in the endoplasmic reticulum of most eukaryotic cells (Phillips and Langdon, 1962; Williams and Kamin, 1962; Lu et al., 1969). It is a 78 kDa membrane-bound flavoprotein, containing one molecule of FMN and one molecule of FAD (Iyanagi and Mason, 1973), which transfers electrons from NADPH via the FMN and FAD prosthetic groups to cytochrome P450. It also has the ability to reduce a number of exogenous electron acceptors, including cytochrome c, and drugs such as mitomycin c, adriamycin and the benzotriazine SR4233 (Williams and Kamin, 1962; Keyse et al., 1984; Walton et al., 1992), and is able to donate electrons to haem oxygenase, to the fatty acid elongation system and to cytochrome b_5. The enzyme has been extensively studied by spectroscopic techniques (see Strobel et al. (1995)), including ^{31}P NMR (e.g. Narayanasami et al. (1992)). Crystallisation of an N-terminal truncated P450 reductase from rat liver has been described (Djordjevic et al., 1995), and the structure has very recently been reported (Kim et al., 1996), although details are not yet available.

P450 reductase is a multidomain protein (Smith et al., 1994; Fig. 1A), having a hydrophobic membrane-anchoring N-terminal region, an FMN-binding domain homologous with the bacterial flavodoxins, and a C-terminal domain homologous with the FAD-containing ferredoxin-

*To whom correspondence should be addressed at: Centre for Mechanisms of Human Toxicity, University of Leicester, P.O. Box 138, Hodgkin Building, Lancaster Road, Leicester LE1 9HN, U.K.

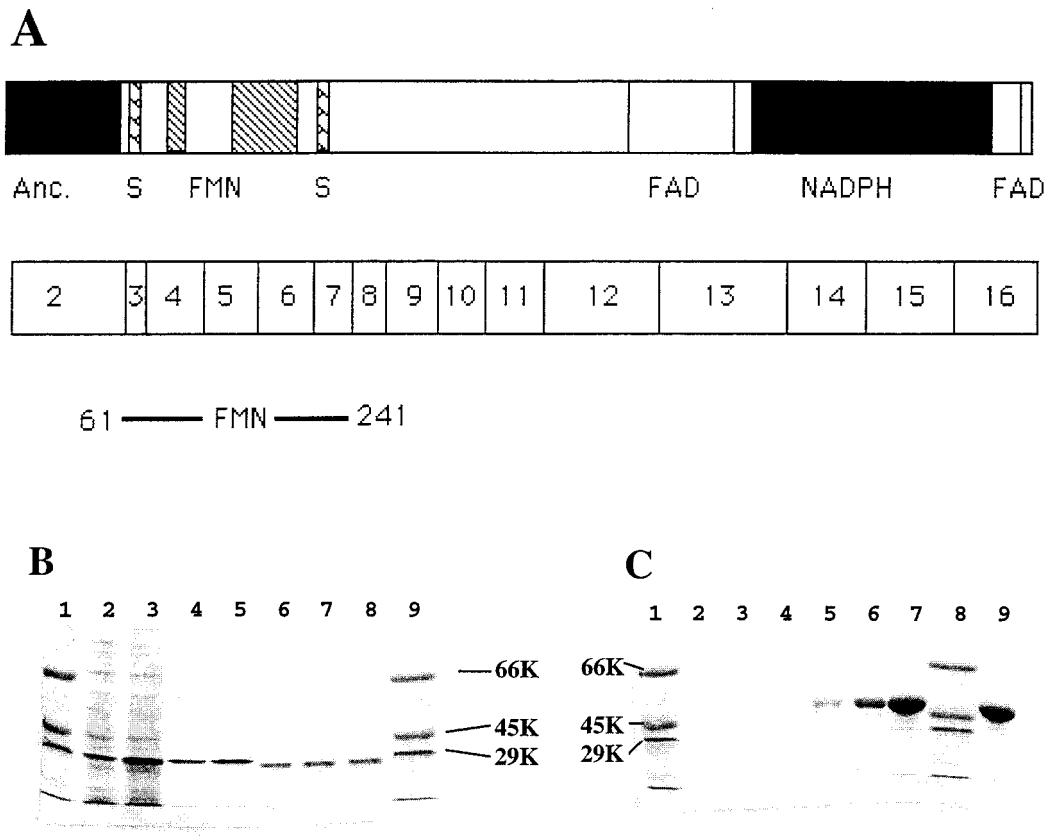

Fig. 1. (A) Organisation of the human cytochrome P450 reductase gene, showing the exon boundaries and the functional regions, including the FMN-, FAD- and NADPH-binding regions, the membrane-anchoring region (Anc.) and the substrate-binding regions (S). The location of the domain made for this study is shown at the bottom. (B) SDS-polyacrylamide gels showing the purification of the FMN domain (exons 3–7). Lanes 1 and 9: molecular weight markers; lane 2: total cell protein before induction; lane 3: total cell protein after induction; lanes 4 and 5: eluent from the first nickel column; lane 6: after proteolysis with thrombin and the second nickel column; lanes 7 and 8: after final purification. Samples with the histidine tag (lanes 4 and 5) run at slightly higher molecular mass than those from which this has been removed by thrombin (lanes 6, 7 and 8). (C) SDS-polyacrylamide gel analysis of the interaction between the FMN domain and the FAD/NADPH domain. The histidine tagged FMN domain (2 mg) was bound to a 2 ml nickel-agarose column, and the FAD/NADPH domain (4.6 mg) was applied in 1 mM potassium phosphate, pH 7.5, and allowed to bind to the immobilised FMN domain. The concentration of the buffer passed through the column was then increased progressively from 1 to 180 mM phosphate. Lanes 2–7 and 9 represent, respectively, fractions eluted with 5, 15, 30, 50, 75, 120 and 180 mM phosphate buffer, pH 7.5. Lanes 1 and 8 show molecular weight markers.

$NADP^+$ reductase (Porter and Kasper, 1986; Porter, 1991). Two other groups of proteins contain both FMN and FAD, and share significant sequence identity with P450 reductase, particularly within the suggested functional domains: nitric oxide synthase and the α subunit of bacterial sulphite reductase (Porter, 1991). Recently, we reported (Zhao et al., 1996) the expression in *E. coli* of separate FMN-binding and FAD/NADPH-binding domains of human P450 reductase (corresponding to exons 3–8 and 8–16, respectively; Fig. 1A). A functional monooxygenase system could be reconstituted using the two recombinant domains together with rat cytochrome P450 1A1. Studies of the individual and the reconstituted domains promise to be valuable in understanding electron transfer through the reductase from NADPH to cytochrome P450. During catalytic turnover with cytochrome P450 as the electron acceptor, microsomal P450 reductase has been proposed to cycle between one-electron and three-electron (or two-electron and four-electron) states (Backes, 1993), with only the two-electron-reduced FMN ($FMNH_2$) being able to donate electrons to the haem of cytochrome P450. On the other hand, it has recently been shown that in the bifunctional *Bacillus megaterium* cytochrome P450 BM3 only the FMN semiquinone ($FMN^{\cdot}$) is capable of reducing the haem iron, the $FMNH_2$ state being inactive in this respect (Sevrioukova and Peterson, 1995; Sevrioukova et al., 1996).

The domain constructs reported earlier (Zhao et al., 1996) were designed on the basis that exons or groups of exons within the P450 reductase gene defined specific functional domains. We now report the expression and characterisation of a somewhat smaller functional FMN domain (exons 3–7, 20.7 versus 24.2 kDa). Using ^{13}C,^{15}N-labelled protein, we have assigned the ^1H, ^{13}C and ^{15}N resonances of the protein backbone and most of those of the side chains. From an analysis of the NMR data, we

have deduced the secondary structure and global fold of this domain and have compared these with the structures of bacterial flavodoxins.

Materials and Methods

Constructs and protein expression

The cDNA for human NADPH-cytochrome P450 reductase was derived from a human skin fibroblast cDNA library as previously described (Smith et al., 1994). PCR amplification using oligonucleotide primers to the 5' and 3' ends of exons 3 and 7 (Fig. 1A) was used to generate the cDNA encoding the FMN domain. The 5' oligonucleotide contained an *Nde I* restriction site and the 3' end oligonucleotide contained an *Xho I* site to enable subcloning into the unique *Nde I*/ *Xho I* sites of the expression vector pET15b (Novagen, Madison, WI, U.S.A.), generating the plasmid pMP used for FMN domain expression. PCR products were cloned into the PCR vector pGEM-T (Promega, Madison, WI, U.S.A.) and sequenced before subcloning into pET15b; pMP contains a silent base pair change (A to G) at nucleotide position 387 which does not affect protein sequence integrity. In pMP, the structural gene for the FMN domain was positioned downstream of a polyhistidine tag (His_6) and a thrombin cleavage site to facilitate purification of the recombinant protein. pMP was transformed into *E. coli* BL21(DE3)-pLysS for expression.

Uniformly ^{15}N-labelled FMN domain was obtained by growing the transformed *E. coli* in 2 × M9 medium containing 1 g/l of [^{15}N]ammonium chloride as the sole nitrogen source, with 50 μg/ml ampicillin and 34 μg/ml chloramphenicol. For uniformly [^{15}N,^{13}C]-labelled protein, the same 2 × M9 medium was used, but with 1.8 g/l ^{13}C-glucose as the sole carbon source. Cultures were grown in 500 ml batches in 2 l flasks shaken at 37 °C. At $A_{600} \sim 0.7$, expression was induced by the addition of IPTG (final concentration 50 μg/ml). After 3–4 h further growth at 37 °C, cells were harvested by centrifugation (16 000 × g, 5 min, 4 °C). Cell pellets were frozen overnight at –20 °C. To prepare selectively ^{15}N-labelled FMN domain, the same *E. coli* strain was grown in a 2 × M9 medium containing a mixture of unlabelled amino acids in the quantities listed by Griffey et al. (1985) to which the appropriate ^{15}N-labelled amino acid (leucine, phenylalanine and tyrosine) was added in approximately the same quantity. These amino acids were the only nitrogen source in the medium. The cells were grown as above, and at the time of induction a second equal amount of the appropriate ^{15}N-labelled amino acid was added.

Protein purification

The larger FMN domain (exons 3–8) and the FAD/NADPH domain (exons 8–16) were expressed and purified as described earlier (Zhao et al., 1996), and the smaller FMN domain was purified in the same way. One litre cultures yielded 50 mg of pure FMN domain. Figure 1B shows the SDS-polyacrylamide gel electrophoresis analysis of each step in the purification. The purified domain was characterised by enzyme assay, electrospray mass spectrometry and N-terminal sequencing. The expression system used leads to the addition of four additional residues (GSHM) at the N-terminus, and sequencing of the FMN domain gave the expected GSHMTSSVRE----.

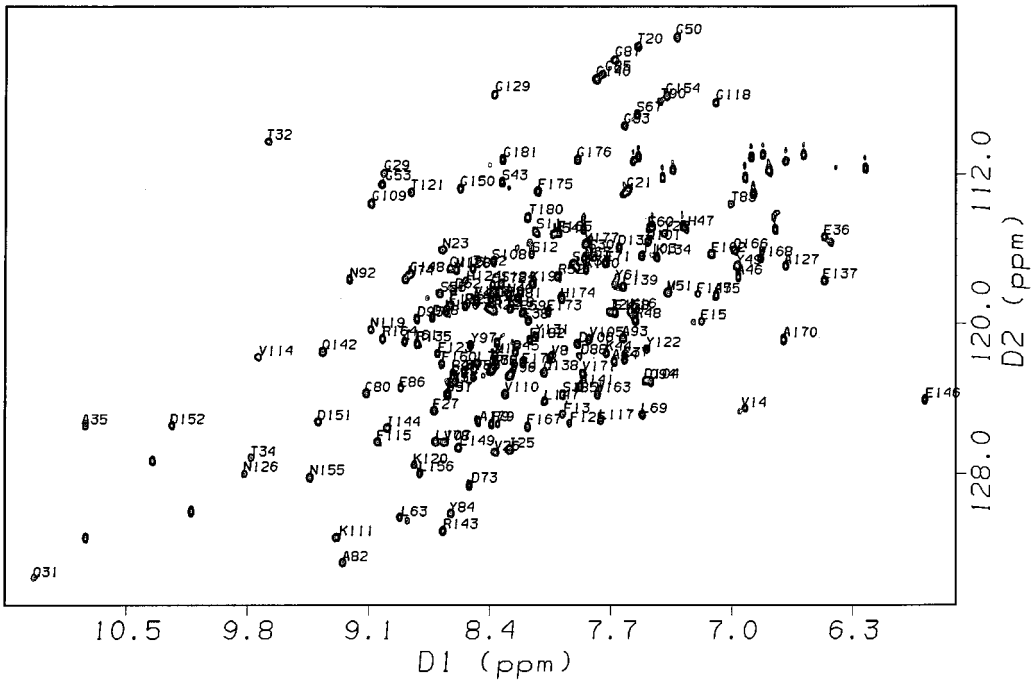

Fig. 2. The ^{15}N,^{1}H HSQC spectrum of the FMN domain. The assignments of backbone amide cross peaks are indicated.

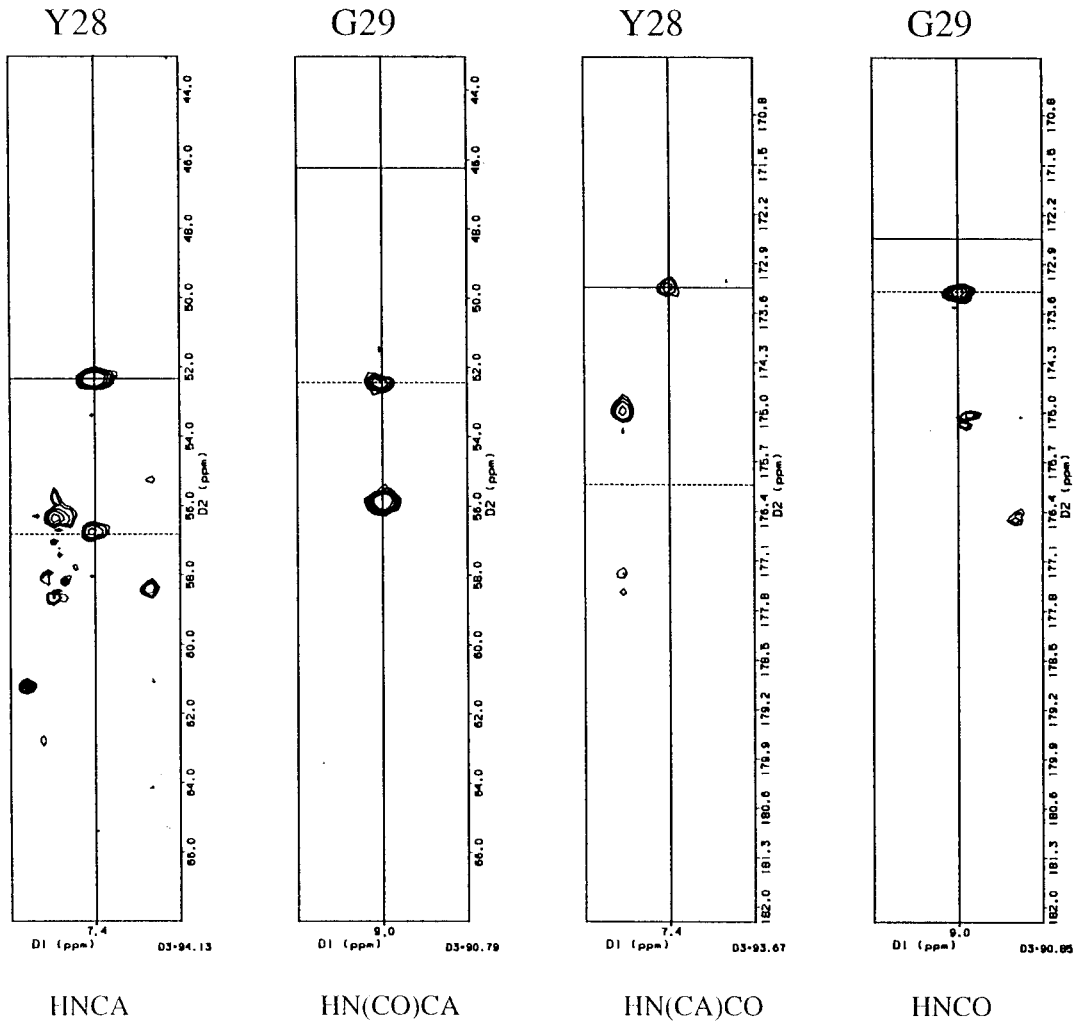

Fig. 3. $^{1}H/^{13}C$ slices from 3D triple-resonance experiments representing sequential connectivities of Tyr[28] and Gly[29]. From left to right, the experiments shown are HNCA, HN(CO)CA, HN(CA)CO and HNCO. Intraresidue cross peaks are marked with solid horizontal lines and sequential cross peaks with dashed horizontal lines.

Preparation of apo-protein

FMN was removed from the protein by a modification of the procedure of Edmondson and Tollin (1971). A 30% (w/v) solution of trichloroacetic acid was added, in the dark at 4 °C, to the FMN domain (0.5 mg/ml) in 40 mM phosphate, pH 6.8, 0.2 mM DTT, 0.02 mM EDTA, 20% glycerol to a final concentration of 3%. The solution was centrifuged (20 000 rpm, JA20 rotor, for 5 min at 4 °C), and the pellet was washed with ice-cold 3% trichloroacetic acid, 1.3 mM DTT in water. The pellet was suspended in 40 mM phosphate, pH 6.8, 1.3 mM DTT, 0.02 mM EDTA, and was dialysed against the same buffer with 0.2 mM DTT.

NMR spectroscopy

Samples for NMR consisted of 0.5–1.2 mM FMN domain in 40 mM phosphate, pH 6.8, 0.2 mM DTT, 0.02 mM EDTA. The purified FMN domain was exchanged into the buffer by ultrafiltration (5K cutoff membrane) or gel filtration (Sephadex G25M, Pharmacia Biotech, Uppsala, Sweden). Unless otherwise stated, all experiments were performed at 298 K on Bruker DMX 500 and AMX 600 spectrometers. Typically, the ^{1}H spectral width was set to 13 ppm with the transmitter offset at the frequency of the water resonance. The ^{15}N spectral widths were 90 ppm for the 2D $^{15}N,^{1}H$ HSQC spectrum and 33 ppm for 3D spectra centred at 119.4 ppm. The ^{13}C spectral widths were 70 ppm for the 2D $^{13}C,^{1}H$ HSQC spectrum centred at 40 ppm; 26.7 ppm centred at 55.9 ppm for 3D experiments involving the detection of $^{13}C^{\alpha}$ resonances; 13.4 ppm centred at 176.6 ppm for 3D experiments involving the detection of ^{13}CO resonances; 66 ppm centred at 43 ppm for 3D experiments involving the detection of $^{13}C^{\alpha}/^{13}C^{\beta}$ resonances; and 70 ppm for 3D and 23.4 ppm for 4D centred at 40 ppm in experiments involving the detection of all non-aromatic ^{13}C resonances. The ^{1}H chemical shifts were referenced to the methyl proton resonance of external DSS, and the ^{15}N and ^{13}C shifts were indirectly

referenced to external DSS. All experiments involving ^{15}N detection (apart from simultaneous ^{15}N,^{13}C-resolved NOESY-HMQC) were performed using a sensitivity-enhanced pulse-field gradient sequence (Kay et al., 1992), which required slight modifications of some of the originally published pulse sequences.

The following 3D triple-resonance experiments were used for the backbone resonance assignments: HNCA (Muhandiram and Kay, 1994; 48 complex points in the ^{13}C dimension), HNCO (Muhandiram and Kay, 1994; 48 complex points in the ^{13}C dimension), HN(CA)CO (Clubb et al., 1992; 48 complex points in the ^{13}C dimension), HN(CO)CA (Grzesiek and Bax, 1992a; 48 complex points in the ^{13}C dimension), CBCANH (Grzesiek and Bax, 1992b; 48 complex points in the ^{13}C dimension), and CBCA(CO)NH (Muhandiram and Kay, 1994; 48 complex points in the ^{13}C dimension); 512 complex points were recorded in the acquisition dimension and 40 complex points in the constant-time ^{15}N dimension. The remaining parameters are described in the corresponding references. Resonances of the side chains were assigned using cross-polarisation 3D HCCH-TOCSY (Majumdar et al., 1993) (512, 128 and 36 complex points in the acquisition, indirect ^{1}H and ^{13}C dimensions, respectively) and 4D HCCH-TOCSY with an additional ^{13}C evolution period added before the mixing time (512, 64, 18 and 18 complex points in the acquisition, indirect ^{1}H and each ^{13}C dimension, respectively). Sequential NOEs were detected in 3D NOESY-HSQC (Zhang et al., 1994) (mixing time 100 ms; 512, 128 and 36 complex points in the acquisition, indirect ^{1}H and ^{15}N dimensions, respectively) and simultaneous ^{15}N,^{13}C-resolved NOESY-HMQC (Pascal et al., 1994) (mixing time 100 ms; 512, 128 and 36 complex points in the acquisition, indirect ^{1}H and heteronuclear dimensions, respectively). Because of the relatively low sample concentration, this last spectrum was recorded on a Bruker DMX 800 spectrometer to obtain the benefit of the greater sensitivity at the higher field. Long-range NOEs were obtained from a 4D ^{1}H,^{13}C HMQC-NOESY-HMQC spectrum (Vuister et al., 1993) (mixing time 100 ms; 512, 64, 18 and 18 complex points in the acquisition, indirect ^{1}H and each ^{13}C dimension, respectively).

NMR data were processed and analysed using Felix95 software (MSI/Biosym, San Diego, CA, U.S.A.). A sine-bell squared window function was used for apodization in all dimensions with a phase shift of 50° in the acquisition and 60–70° in the indirect dimensions. Linear prediction was used to double the number of points in both the heteronuclear and the ^{1}H dimensions of 4D spectra. Cross peaks were picked automatically using the Felix peak-picking routine; peaks from noise or spectral artefacts were removed manually.

Resonance assignment procedure

Backbone resonances were assigned by correlating cross peaks in the six triple-resonance experiments men-

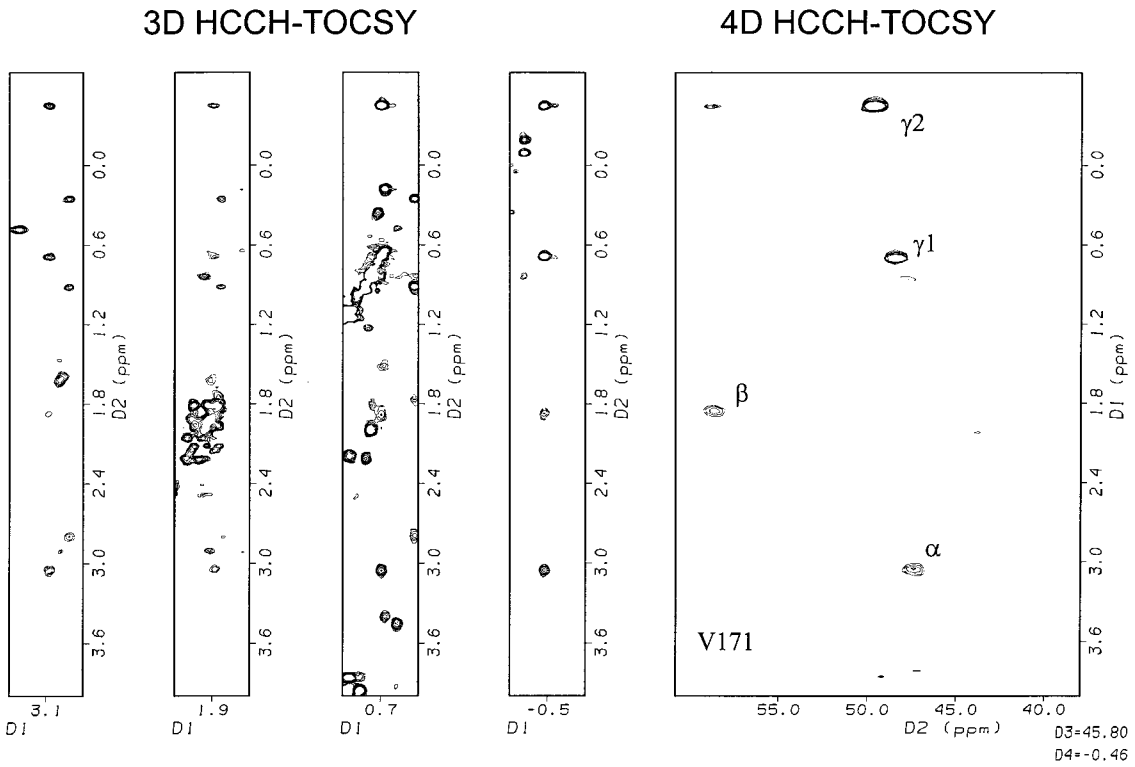

Fig. 4. Comparison of slices from a 3D HCCH-TOCSY spectrum and a plane from a 4D HCCH-TOCSY spectrum containing side-chain cross peaks of Val[171].

Fig. 5. Information on the secondary structure of the FMN domain obtained from NMR. From bottom to top: the sequences of the FMN domain (P450R) and of *D. vulgaris* flavodoxin (D.v. fvd), aligned as used for the model building; slowly exchanging amide protons, represented by filled circles; sequential and intraresidue NOEs (the intensity is represented by the height of the bar; asterisks indicate NOEs not observed because of resonance overlap or missing assignments); the consensus chemical shift index; and the secondary structure of *D. vulgaris* flavodoxin.

tioned above (HNCA, HNCO, HN(CA)CO, HN(CO)CA, CBCANH, CBCA(CO)NH) in the conventional manner. Programs were developed in-house for a semiautomated approach to the assignment process, and these will be described in detail elsewhere (K.H. Sze, I. Barsukov, L.-Y. Lian and G.C.K. Roberts, in preparation). Briefly, cross peaks were grouped into peak systems on the basis of ^{15}N and ^{1}H chemical shifts, and these peak systems were linked into fragments on the basis of sequential links between them obtained from the triple-resonance experiments. These fragments (and the peak systems which could not be linked in fragments) were correlated with the primary sequence on the basis of residue type as defined by $^{13}C^{\alpha}$ and $^{13}C^{\beta}$ chemical shifts (Friedrichs et al., 1994). Additional information on the residue type of the peak systems was obtained from $^{15}N,^{1}H$ HSQC spectra of protein selectively labelled with ^{15}N at leucine, phenylalanine or tyrosine residues. Ambiguities were resolved by a simulated annealing procedure (K.H. Sze, I. Barsukov, L.-Y. Lian and G.C.K. Roberts, in preparation), and the assignments were checked manually at each step.

Spin systems of the aliphatic side chains were identified in 3D and 4D HCCH-TOCSY spectra. Cross peaks from 3D HCCH-TOCSY spectra were first combined into peak strips on the basis of the ^{1}H and ^{13}C chemical shifts of CH groups, and the strips were then combined into spin systems using the ^{1}H chemical shifts in the indirect proton dimension. In the 4D HCCH-TOCSY experiment cross peaks were extracted from the 2D planes at the ^{1}H and ^{13}C chemical shifts of CH groups.

Deuterium exchange

The protein was transferred into D_2O buffer by three 10-fold dilution/concentration steps at 4 °C, taking ~6 h to complete. Cross peaks observed in a $^{1}H,^{15}N$ HSQC spectrum obtained immediately after this transfer were considered to correspond to slowly exchanging protons.

Structural modelling

A model based on the NMR data and on homology with *Desulfovibrio vulgaris* flavodoxin (Watt et al., 1991; PDB entry 2fx2) was calculated using MODELLER 3.0 (Sali and Blundell, 1993). NMR data were introduced as restraints on secondary structure with the HELIX, STRAND and SHEET options of the program. Long-range NOEs were converted into upper-limit distance restraints as follows. The restraints were applied to carbon atoms in such a way that the upper limit on the distance between interacting protons was 4 Å. This involved adding 1 Å for each chemically unique group. In the case of the methyl groups of valine and leucine, the restraint was applied to the C^{β} or C^{γ} atom, respectively, with 2 Å added in each case. If NOEs were observed for both methyl groups to the same proton, each of the groups was restrained separately in the same way as for chemically unique groups.

Results and Discussion

Design, expression and characterisation of the FMN domain

The design of the FMN domain was based on the premise that exons within the reductase gene (Fig. 1A)

define a specific functional domain (Smith et al., 1994). Exons 4–6 show the highest homology with the flavodoxin from *D. vulgaris*, but a protein corresponding to exons 4–6 does not bind flavin (Smith et al., 1994) while one corresponding to exons 3–8 is fully functional (Smith et al., 1994; Zhao et al., 1996). We therefore made a construct corresponding to exons 3–7 (residues 61–241); high levels of expression of predominantly soluble recombinant protein were achieved in *E. coli* and the domain was purified to homogeneity (see Materials and Methods, and Fig. 1B). The UV/visible absorption spectrum of the FMN domain had maxima at 370 and 453 nm and was virtually identical to that of FAD-depleted P450 reductase (Kurzban et al., 1990). The purified FMN domain, after the ion exchange step, contained 0.98 mol of flavin per mol of protein, identified as FMN by NMR after denaturation of the protein sample by boiling. Thus, this FMN domain construct (exons 3–7) is able to fold independently and to bind FMN. As a further test for the function of this domain, we investigated its ability to bind the FAD/NADPH-binding domain and to accept electrons from it.

The FMN domain with its histidine tag still attached was bound to a nickel-agarose column. The purified FAD/NADPH domain (without the histidine tag) was found to bind tightly to the column in 1 mM phosphate buffer, pH 7.0, and to be eluted by increasing the ionic strength (Fig. 1C); as a control, the FAD/NADPH domain was shown not to bind to the nickel-agarose column in the absence of the FMN domain. This behaviour is the same as that observed with the larger FMN domain construct (exons 3–8), and similarly it was shown that both FMN domain constructs were able to bind cytochrome c. When the FMN domain and the FAD/NADPH domain were mixed together in solution and excess NADPH was added, a spectrum characteristic of the FMN semiquinone form of native P450 reductase was obtained, which was stable for at least 4 h. This demonstrates that the FAD/NADPH domain can transfer electrons to the smaller FMN domain (exons 3–7), to produce an air-stable semiquinone, as seen in native P450 reductase. Thus, the smaller FMN domain is able to fold independently, to bind FMN and to interact functionally with the FAD/NADPH domain.

Resonance assignment

The ^{15}N HSQC spectrum of the shorter FMN domain (Fig. 2) has better resolution than that of the larger construct (not shown), but the resolution is still insufficient for a straightforward grouping of cross peaks into peak systems of intraresidue and sequential peaks using only ^{15}N-labelled protein. We therefore prepared [^{13}C,^{15}N]-labelled protein and made the resonance assignments on the basis of 3D triple-resonance spectra (see Materials and Methods). The sensitivity of the triple-resonance spectra was sufficient to allow us to identify most of the expected cross peaks; an example is shown in Fig. 3. In

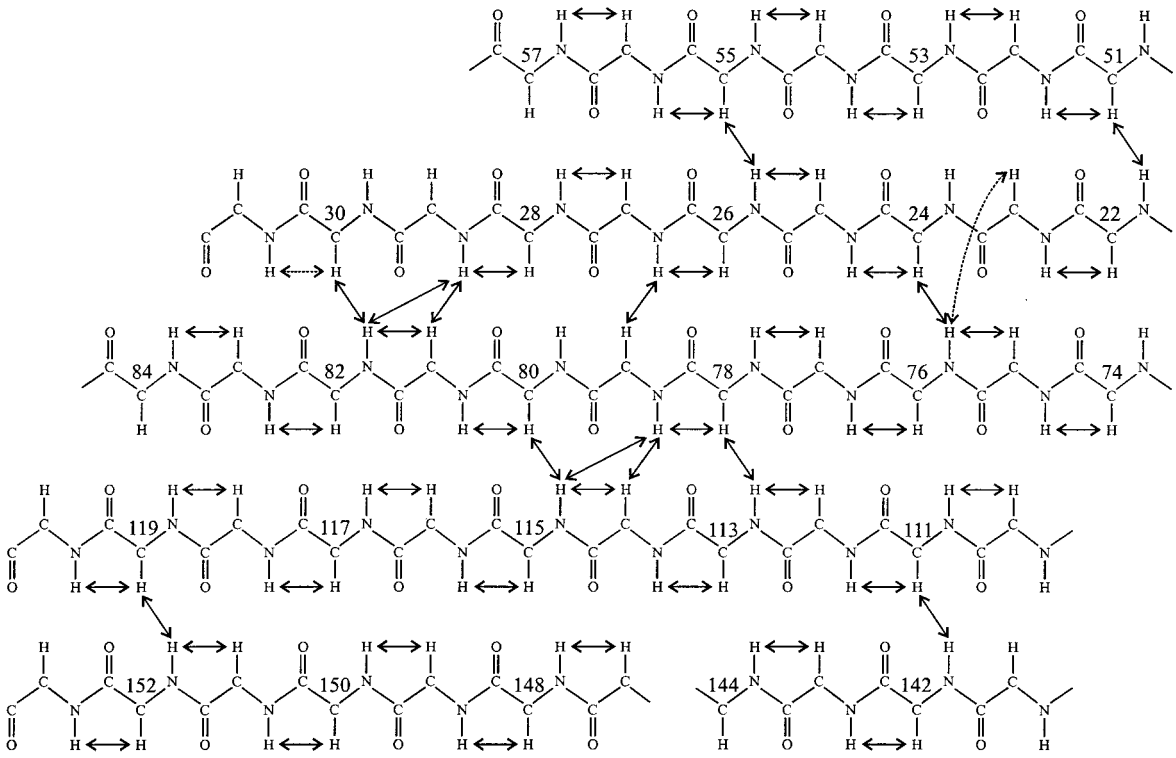

Fig. 6. Schematic representation of the NOEs used to deduce the ordering and alignment of the β-strands. Uniquely assigned NOEs are shown as arrows. Dashed arrows represent low-intensity NOEs.

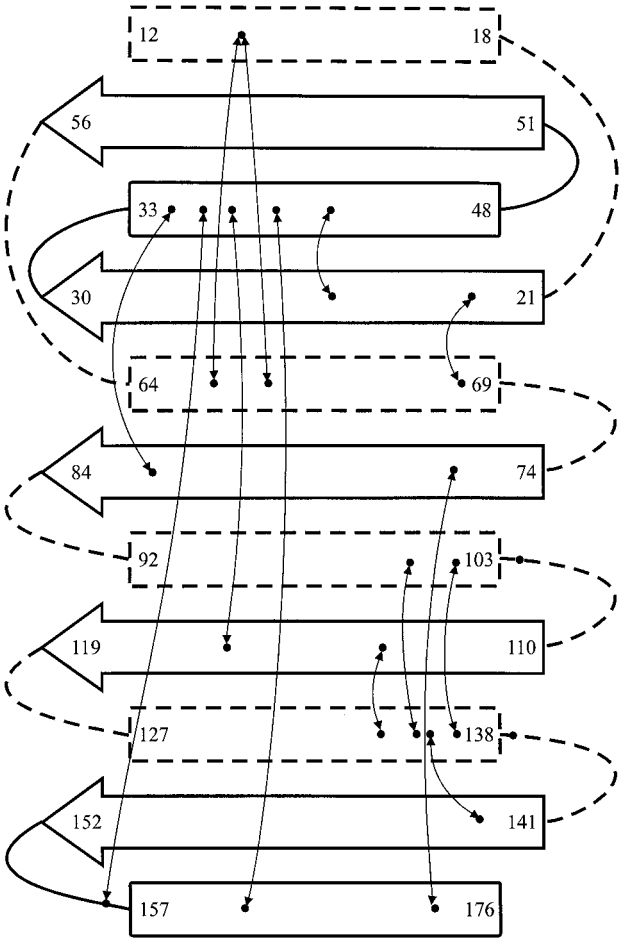

Fig. 7. Schematic representation of the topology of the FMN domain as deduced from long-range NOEs. β-Strands are represented by arrows and helices by rectangles. Helices above the plane are drawn in solid lines and those below the plane in dashed lines. Helix–helix and helix–sheet NOE connectivities are shown as arrows; connectivities between β-strands (cf. Fig. 6) are omitted for clarity.

the least sensitive experiments, HN(CA)CO and CBCA-NH, approximately 50% and 40%, respectively, of the expected cross peaks were identified, while the HNCA, HNCO and HN(CO)CA spectra contained nearly 100% of the expected cross peaks. This provided enough information to perform the assignment.

A number of systems of intense cross peaks were found to have a 'shadow' peak system of low-intensity peaks, with similar ^{13}C chemical shifts and a small but significant difference in ^{15}N and/or $^{1}H^{N}$ chemical shifts. The sequential connectivities of these peaks followed the same pattern and during the assignment procedure minor and major systems were 'competing' for the same positions at the C-terminus of the protein sequence. The minor peak systems were disregarded at this stage. These observations indicated the simultaneous presence of two forms of protein, affecting residues 175–185 at the C-terminus. In the absence of any evidence from mass spectrometry for chemical heterogeneity of the protein, we presume that there is a minor conformation (~10%) in this part of the structure.

Resonances from all the non-proline residues were assigned, except for seven at the N-terminus. Five peak systems with relatively weak cross peaks are left unassigned due to the absence of reliable sequential connections. Some of these may arise from the minor conformation of the protein. An inspection of the $^{15}N,^{1}H$ HSQC spectrum (Fig. 2) shows no strong cross peaks that were not assigned. The most intense peaks in this spectrum correspond to 10 C-terminal residues, whose chemical shifts are close to the values expected for random-coil conformation; this suggests that this part of the structure is mobile in the major conformation.

Side-chain spin systems were identified in 3D and 4D HCCH-TOCSY spectra (see Materials and Methods). The 4D HCCH-TOCSY was found to be superior to the 3D version of the experiment in the case of residues containing methyl groups (threonine, valine, isoleucine, leucine). For most of such residues the resonance of at least one methyl group is usually resolved in the $^{13}C,^{1}H$ HMQC spectrum, and the corresponding plane from the 4D spectrum shows cross peaks for all CH groups of the residue, as illustrated in Fig. 4. Thus, all the ^{13}C and ^{1}H chemical shifts of the spin system can be deduced from a single plane of the 4D spectrum, while obtaining ^{13}C chemical shifts using the 3D spectrum requires the correlation of several strips (Fig. 4). In the 4D spectrum, well-resolved spin systems can also be found in planes at $^{13}C^{\alpha},^{1}H^{\alpha}$ chemical shifts which are well separated in the $^{13}C,^{1}H$ HMQC spectrum. On the other hand, the low digital resolution of the 4D spectrum does not allow a clear identification of cross peaks of residues with long side chains, and a combination of 3D and 4D spectra was therefore used. The sensitivity of the 4D spectrum was found to be very close to that of the 3D spectrum, and most of the cross peaks identified in the 3D spectrum could also be found in the 4D spectrum. The spin systems from HCCH-TOCSY spectra were correlated with the backbone resonances on the basis of ^{1}H and ^{13}C resonances of $C^{\alpha}H$ and $C^{\beta}H$ groups. The number of chemical shifts available for correlation (up to four) was sufficient for unambiguous side-chain assignments. The ^{1}H, ^{13}C and ^{15}N assignments are given in the supplementary material, and have been submitted to the BioMagRes Bank.

Secondary structure and global fold

Regions of regular secondary structure can be identified from an analysis of the deviation of the experimental ^{1}H and ^{13}C chemical shifts from random-coil values (the chemical shift index; Wishart and Sykes, 1994), the intensity distribution of the intraresidue and sequential NOEs involving H^{N} protons, and the hydrogen exchange rates. These data for the FMN domain are summarised in Fig. 5. Six helical regions separated by five regions of ex-

tended structure can be readily identified. The consensus chemical shift index correlates well with the NOE data. Residues with a chemical shift index corresponding to helix formation show strong H_i^N/H_{i-1}^N and $H_i^N/C^\alpha H_i$, as well as weak $H_i^N/C^\alpha H_{i-1}$, NOE connectivities, while residues in the extended regions have strong sequential $H_i^N/C^\alpha H_{i-1}$ and weak or absent H_i^N/H_{i-1}^N and $H_i^N/C^\alpha H_i$ NOE connectivities. For most of the β-strands, the continuous stretches of characteristic NOEs extend beyond the C-terminal limit of the chemical shift index. The first strand, β1, has a distortion in its N-terminal part at residue Ile^{24} as indicated by the observation of a strong H_i^N/H_{i-1}^N cross peak, and an analogous break in the NOE connectivity pattern is observed in the last strand, β5, at Phe^{145}. Most of the slowly exchanging H^N protons are in the regions of regular secondary structure. Some of the secondary structure elements have no slow exchanging H^N protons (by the qualitative criterion used – see Materials and Methods), indicating a lower kinetic stability.

The arrangement of the β-strands into a β-sheet was deduced from a number of interstrand NOEs assigned by the simultaneous analysis of 3D ^{15}N- and ^{13}C-separated spectra (see Materials and Methods). The interstrand NOEs involving H^N protons are indicated in Fig. 6. At least two interstrand NOEs have been identified between each pair of neighbouring strands. These interstrand connections show that the β-sheet is parallel, as might be expected from the alternation of strands and helices along the sequence (Fig. 6). The three central β-strands contain slowly exchanging amide groups, and form a stable core of the protein, while no slowly exchanging amide groups have been identified for the external strands β2 and β5, indicating their higher accessibility to bulk water. The observation of interstrand NOEs from Leu^{76} H^N to the $C^\alpha H$ of both Asn^{23} and Ile^{24} confirms the distortion of strand β1 at position 24 indicated by the sequential NOEs. The last strand, β5, has a frame shift of one or two residues around position 144, as evidenced by the disruption of the sequential NOE pattern.

Once the topology of the β-sheet had been identified, the approximate positions of the α-helices could be determined from a set of unambiguously assigned long-range NOEs in the 4D ^{13}C-separated HMQC-NOESY-HMQC spectrum. The majority of these NOEs involve at least one methyl group, and were easily assignable due to the relatively strong and well-resolved signals from these groups. The NOEs observed between the residues in helices and the rest of the protein are shown schematically in Fig. 7. (For clarity, the side-chain to side-chain NOEs observed between β-strands are not shown in the figure, but were in agreement with the strand positions indicated in Fig. 6.) The NOE analysis demonstrates an interaction between helices α2 (residues 33–48) and α6 (157–176). These helices must thus be packed against one face of the β-sheet, while helices α4 (92–103) and α5 (127–138) are packed against the other face. The short helix α3 (64–69) is on the same side of the β-sheet as α4 and α5, as shown by its contacts with the β-sheet. This allows the polypeptide chain to make a connection between strands β2 and β3 without crossing over helix α2. Helix α1 makes a contact to helix α3. The topology of the FMN domain deduced from the long-range NOEs and shown in Figs. 6 and 7 agrees with the general rules for the topology of α/β proteins.

Comparison to homologous proteins

The sequence homology of the FMN-binding domain of P450 reductase to bacterial flavodoxins has long been recognised (Porter and Kasper, 1986), and the X-ray and NMR structures of a number of flavodoxins from different species are available (e.g. Burnett et al. (1974), Watt et al. (1991), Fukuyama et al. (1992), Rao et al. (1992), Stockman et al. (1993), Knauf et al. (1996), Peelen et al. (1996) and Romero et al. (1996) and references cited therein). The sequence of the FMN domain aligns most closely with that of the flavodoxin from *D. vulgaris*, and we have therefore used this protein for the comparison. The positions of the regular secondary structure elements of *D. vulgaris* flavodoxin, as shown in Fig. 5, are gen-

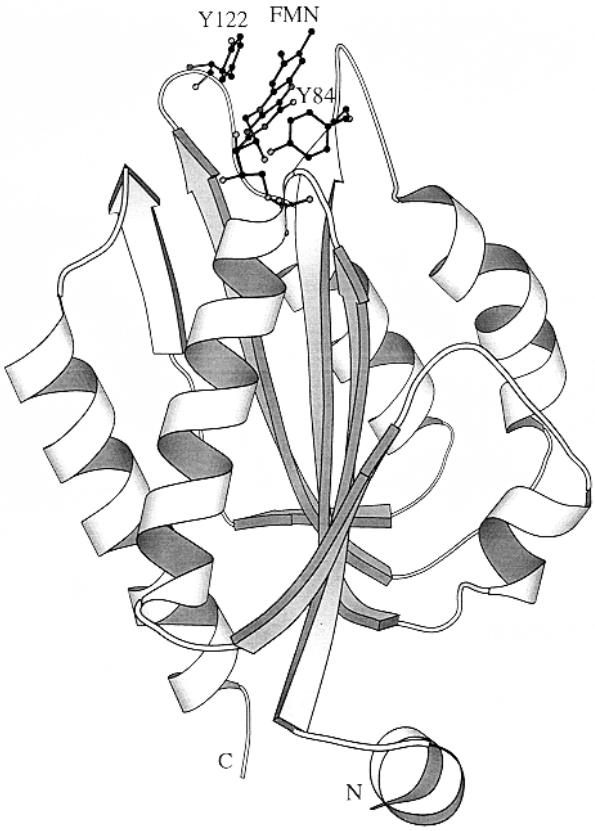

Fig. 8. MOLSCRIPT representation of the 3D structure of the FMN-binding domain of cytochrome P450 reductase, based on the NMR constraints and on homology with *D. vulgaris* flavodoxin. The FMN and the side chains of Tyr^{84} and Tyr^{122} are shown in ball-and-stick representation.

erally in good agreement with those of the FMN domain, but there are a few notable differences. The stretch of residues corresponding to the short helix α3 in the FMN domain has not been identified as an α-helix in the flavodoxin structure, although the corresponding residues do have a broadly helix-like conformation in the latter case. The C-terminal part of this helix corresponds to the only insertion in the sequence of the FMN domain relative to that of the flavodoxin in the alignment used. The last β-strand of flavodoxin has a kink at the position corresponding to the observed strand distortion in the FMN domain (Phe[145]); longer chain flavodoxins have an insertion at this position, forming a loop which connects two parts of the β-strand. With the alignment used (Porter and Kasper, 1986), the FMN domain is longer than the flavodoxins at both the N- and C-termini. The C-terminal helix is longer by about one turn in the FMN domain; in the intact reductase, this leads to a linker region between the FMN and FAD/NADPH domains. An additional helix is formed at the N-terminus of the FMN domain, which may be required for the correct relative orientation of the anchor and FMN domains in the intact reductase.

The similarity between the general fold of the FMN domain deduced from NOE analysis and that of flavodoxin allowed us to combine the NMR constraints with homology modelling to generate a model of the global fold of the domain using the program MODELLER 3.0 (Sali and Blundell, 1993). The residues in the defined elements of secondary structure shown in Figs. 5–7 were additionally restrained to the corresponding backbone conformations and the relative positions of the β-strands shown in Fig. 6 were fixed by distance restraints between backbone N and O atoms of interacting strands. The long-range NOEs shown in Fig. 7 were represented by 28 upper-limit distance restraints (see Materials and Methods). The model structure is shown in Fig. 8. None of the NOE distance restraints were violated by more than 1 Å, and the secondary structure elements and the relative positions of β-strands were reproduced. The position of the N-terminal helix is not well defined due to an insufficient number of NOE restraints and the lack of homology data. The details of the structure must await further refinement using a much larger number of experimental restraints, but there are already enough data to conclude that the global fold of the protein is as shown in Fig. 8.

FMN binding

The key features of FMN binding seen in flavodoxin are reproduced by the model of the FMN domain. FMN binds in the shallow grove at the C-terminal edge of the β-sheet. The isoalloxazine ring interacts with residues in loops 84–92 and 119–127 and is flanked by the aromatic rings of Tyr[84] and Tyr[122] at the C-terminal ends of strands β3 and β4, respectively. The negatively charged phosphate group is bound by the residues in the loop Ser(30)-Gln-Thr-Gly-Thr-Ala(35) at the N-terminus of helix α2. In the flavodoxin structure, the side-chain hydroxyl and backbone amide groups of the corresponding residues form a number of hydrogen bonds to the phosphate group of FMN. The formation of these hydrogen bonds leads, in flavodoxin, to low-field shifts of the amide proton resonances and the observation of slowly exchanging hydroxyl protons with chemical shifts in the range 6–8 ppm (Peelen and Vervoort, 1994). We observed similar low-field shifts

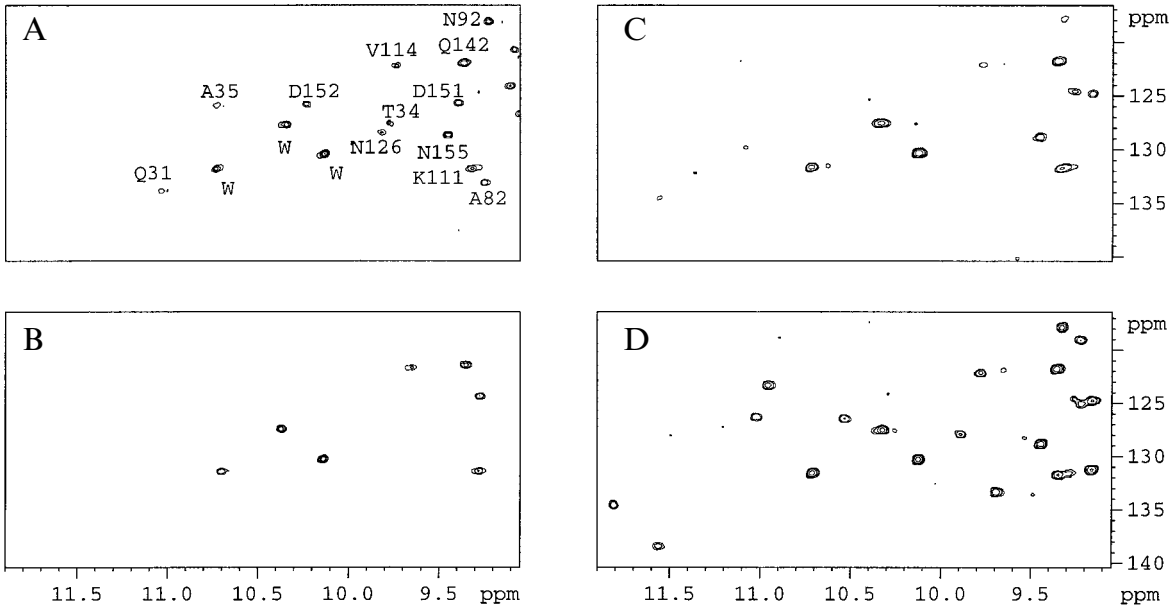

Fig. 9. Parts of the $^{15}N,^{1}H$ HSQC spectrum of the FMN domain (A) in its complex with oxidised FMN, (B) in the apo form, (C) in its complex with the semiquinone form of FMN, and (D) in its complex with the hydroquinone form of FMN.

TABLE 1
CHANGES IN THE ^{15}N HSQC SPECTRUM UPON FMN REDUCTION AND REMOVAL

Residue	Apo-protein	Semiquinone	Hydroquinone
Gln^{31}	s	b	s
Thr^{32}	s	b	s
Ala^{35}	s	b	s
Lys^{44}	s	ss	ss
Gly^{50}	ss	–	–
Ala^{64}	s	–	–
Ser^{67}	ss	–	–
Cys^{80}	s	b	s
Ala^{82}	s	b	s
Tyr^{84}	s	b	s
Glu^{86}	s	b	s
Gly^{87}	s	b	s
Thr^{90}	s	b	s
Asn^{92}	s	b	s
Ala^{93}	s	b	ss
Asp^{95}	s	–	–
Tyr^{97}	s	b	s
Asp^{98}	s	ss	ss
Lys^{111}	ss	ss	ss
Leu^{117}	s	b	ss
Gly^{118}	s	b	ss
Asn^{119}	s	b	s
Thr^{121}	s	b	s
Asn^{126}	s	b	s
Ala^{127}	s	b	s
Gly^{129}	s	b	s
Glu^{146}	s	ss	ss
Leu^{149}	ss	b	ss
Gly^{150}	s	b	s
Asp^{151}	s	b	s
Asp^{152}	s	b	s
Gly^{154}	s	b	s
Asn^{155}	s	b	ss
Trp^{163}	s	–	–

Spectral changes are represented by symbols as follows: s – chemical shift change >0.05 ppm in ^{1}H and/or >0.5 ppm in ^{15}N; ss – small chemical shift change, <0.05 ppm in ^{1}H and <0.5 ppm in ^{15}N; b – signal broadening, resulting in disappearance of the signal in the $^{15}N,^{1}H$ HSQC spectrum. All changes are relative to the holo-protein containing oxidised FMN.

of the amide protons of the phosphate-binding loop but have not detected hydroxyl proton signals in the reported range. In the 2D NOESY spectrum of the doubly labelled FMN domain sample in H_2O, recorded using the WATERGATE (Piotto et al., 1992) method with no water presaturation and no ^{13}C decoupling in the indirect dimension, the only singlet cross peaks observed appear at the water chemical shift in the indirect dimension. As the carbon-bound protons have a doublet structure due to unsuppressed coupling, these singlets should correspond to hydroxyl protons from side chains or water molecules. The coincidence of the hydroxyl chemical shifts with that of the bulk water indicates relatively fast proton exchange for these protons. Thus, in the FMN domain we are able to confirm the formation of hydrogen bonds between the phosphate group and the backbone NH groups, while the hydrogen bonds to the hydroxyl groups of Ser^{30} and Thr^{32}, if formed at all, are weaker than in flavodoxin.

The tight binding of FMN ($K_D = 2.0 \times 10^8\ M^{-1}$) means that unfolding and refolding the protein is the only way to obtain the apo form; this can, however, be achieved with high yield, the removal of FMN being checked optically. The $^{15}N,^{1}H$ HSQC spectrum of the apo form (the low field part of which is shown in Fig. 9B) corresponds to a monomeric protein in a single stable conformation. Upon addition of free FMN, the spectrum becomes identical to the spectrum of the original holo-protein (Fig. 9A). A comparison of the spectra of the apo form and the complex shows a limited number of specific changes in signal positions (Table 1), involving resonances from residues in the FMN-binding loops 31–35, 80–97, 117–129 and also in loop 149–155 which is close to the FMN binding site. The H^N signals from the phosphate-binding loop 31–35 are no longer shifted to low field (Fig. 9B), presumably due to the absence of the strong hydrogen bonds to the phosphate group. Chemical shift changes are also observed for the backbone signals of Ala^{64} from the N-terminal part of helix α3 located at the FMN binding edge of the β-sheet. Thus, all the spectral changes on FMN binding can be attributed either to direct effects of the ligand or to possible local structural changes affecting residues spatially close to the binding site. The overall structure of the protein remains unchanged in the apo form. X-ray crystallographic studies of the apo form of flavodoxin (Genzor et al., 1996) showed that the main effect of FMN removal is a reorientation of the aromatic ring of a tryptophan residue which shields the isoalloxazine ring from solvent so as to fill the cavity left by the FMN removal. The phosphate-binding loop appears to preserve its conformation, although, as noted by Genzor et al. (1996), this may be a result of the presence of inorganic phosphate during crystallisation.

Effects of FMN reduction

The isoalloxazine ring of FMN is normally present in the domain in the oxidised state; it can be reduced by the addition of controlled amounts of dithionite, first to the one-electron-reduced semiquinone state, and further to the two-electron-reduced hydroquinone. Both reduced states are stable for several days under anaerobic conditions. In the semiquinone state the isoalloxazine ring is paramagnetic and uncharged, while in the hydroquinone state it has a negative charge; in both reduced states the ring is protonated on N5.

Titration of the FMN domain with small amounts of dithionite leads to a number of changes in the ^{15}N-resolved HSQC spectra, affecting resonances from approximately 29 residues; these are illustrated in Figs. 9C and D and are summarised in Table 1. As dithionite is first added, a group of 23 backbone cross peaks decrease in

intensity with increasing dithionite concentration. These have largely disappeared by a dithionite:protein ratio of 2:1, at which point the FMN is predominantly in the semiquinone form. In addition, for four well-resolved signals a second component appears alongside the main peak as the titration begins; the intensity of this second component increases with increasing dithionite concentration, while that of the main component decreases. This transfer of intensity to the second component is complete by a dithionite:protein ratio of 2:1, and the new peaks thus can be attributed to signals from the semiquinone form of the FMN domain.

The marked decrease in intensity of some cross peaks in the spectra of the semiquinone form of the protein can be attributed to a paramagnetic broadening of signals from residues close to the isoalloxazine ring. The residues whose signals are affected in this way are in four well-defined regions of the sequence: 31–35, 80–97, 117–129 and 149–155. The first three regions are involved directly in FMN binding (see above). Residues 149–155 form a loop between strand β5 and helix α6 at the same edge of the β-sheet; they do not interact directly with FMN, but the model shows they are close to the isoalloxazine ring, consistent with the observed paramagnetic broadening. By contrast, the resonances which exhibit no broadening, but rather a chemical shift change, correspond to residues which are spatially remote from the isoalloxazine ring but whose environment is altered by reduction of the FMN. The small changes in chemical shift indicate only a slight change in the environment of these residues. Two of the residues affected are in the middle of α-helices and the other two are close to the N-terminal edge of the β-sheet.

At a dithionite:protein ratio of 2:1, two low-intensity cross peaks were observed at positions which did not correspond to any of the protein signals assigned to the oxidised or semiquinone states. The intensity of these signals increased substantially when the dithionite:protein ratio was increased to 6:1, and they thus arise from the hydroquinone state of the protein, present at low concentration at the lower dithionite concentration. At the higher dithionite concentration, a further 18 cross peaks appeared at positions not corresponding to any of the signals of the oxidised protein, while five peaks reappeared close to the positions of oxidised protein signals. Thus, the majority of the signals broadened in the semiquinone state are shifted in the hydroquinone state. No additional signals with a substantial shift in the hydroquinone state have been detected. Thus, the observed chemical shift changes must arise from a direct effect of the negative charge of the isoalloxazine ring or from very localised structural changes. These observations agree with the results of crystallographic studies of different oxidation states of *D. desulfuricans* (Romero et al., 1996) and *D. vulgaris* (Watt et al., 1991) flavodoxins. The main structural change reported is the flip of the Gly-Met peptide bond in the first isoalloxazine ring binding loop upon reduction in such a way that a hydrogen bond is formed between backbone CO and the protonated N5H group of the isoalloxazine. This peptide bond corresponds to residues Gly^{85}–Glu^{86} in the FMN domain, and a shift is indeed observed for the amide cross peak of Glu^{86} on going from the oxidised to the hydroquinone state of the FMN domain. The rest of the structure of the flavodoxins remained virtually the same in the crystal for different oxidation states, again consistent with the very limited changes seen in the spectra of the FMN domain.

The simultaneous observation of cross peaks from the oxidised and semiquinone forms, and from the semiquinone and hydroquinone forms, indicates that electron exchange in the FMN domain is slow on the chemical shift time scale under these solution conditions. This is in contrast to the fast exchange between different oxidation states reported for *D. vulgaris* flavodoxin (Peelen and Vervoort, 1994).

Conclusions

For the FMN-binding domain of human cytochrome P450 reductase, the identification of the elements of secondary structure and of a number of long-range NOEs, leading to a definition of the global fold, have confirmed the general structural similarity of this domain to bacterial flavodoxins, which was expected on the basis of sequence comparisons. Of the two additional α-helices in the reductase domain relative to *D. vulgaris* flavodoxin, the N-terminal helix may have a functional role in the intact enzyme in determining the orientation relative to the membrane-bound anchor sequence. The resonance assignments and structural information reported here provide the groundwork for studies, currently in progress, of the interaction of this domain with its electron transfer partner, cytochrome P450.

Acknowledgements

This work was supported by the Medical Research Council and the Wellcome Trust. We are grateful to the European Union, Prof. H. Rüterjans and Dr. R. Boelens for access to the NMR Large Scale Facilities at the University of Frankfurt, Germany, and the University of Utrecht, The Netherlands.

References

Backes, W.L. (1993) *Handbook Exp. Pharmacol.*, **105**, 15–34.

Burnett, R.M., Darling, G.D., Kendall, D.S., LeQuesne, M.E., Mayhew, S.G., Smith, W.W. and Ludwig, M.L. (1974) *J. Biol. Chem.*, **249**, 4383–4392.

Clubb, R.T., Thanabal, V. and Wagner, G. (1992) *J. Magn. Reson.*, **97**, 213–217.

Djordjevic, S., Roberts, D.L., Wang, M., Shea, T., Camitta, M.G.W.,

Masters, B.S.S. and Kim, J.J.P. (1995) *Proc. Natl. Acad. Sci. USA*, **92**, 3214–3218.
Edmondson, D.E. and Tollin, G. (1971) *Biochemistry*, **10**, 124–132.
Friedrichs, M.S., Mueller, L. and Wittekind, M. (1994) *J. Biomol. NMR*, **4**, 703–726.
Fukuyama, K., Matsubara, H. and Rogers, L.J. (1992) *J. Mol. Biol.*, **225**, 775–789.
Genzor, C.G., Perales-Alcón, A., Sancho, J. and Romero, A. (1996) *Nat. Struct. Biol.*, **3**, 329–332.
Griffey, R.H., Redfield, A.G., Loomis, R.E. and Dahlquist, F.W. (1985) *Biochemistry*, **24**, 817–822.
Grzesiek, S. and Bax, A. (1992a) *J. Magn. Reson.*, **96**, 432–440.
Grzesiek, S. and Bax, A. (1992b) *J. Magn. Reson.*, **99**, 201–207.
Iyanagi, T. and Mason, H.S. (1973) *Biochemistry*, **13**, 1701–1710.
Kay, L.E., Keifer, P. and Saarinen, T. (1992) *J. Am. Chem. Soc.*, **114**, 10663–10665.
Keyse, S.R., Fracasso, P.M., Heimbrook, D.C., Rockwell, S., Sligar, S.G. and Sartorelli, A.C. (1984) *Cancer Res.*, **44**, 5638–5643.
Kim, J.J.P., Wang, M., Roberts, D.L., Paschke, R., Shea, T. and Masters, B.S.S. (1996) *XIth International Symposium on Microsomes and Drug Oxidation*, University of California, Los Angeles, CA, U.S.A.
Knauf, M.A., Löhr, F., Blümel, M., Mayhew, S.G. and Rüterjans, H. (1996) *Eur. J. Biochem.*, **238**, 423–434.
Kurzban, G.P., Howarth, J., Palmer, G. and Strobel, H.W. (1990) *J. Biol. Chem.*, **265**, 12272–12279.
Lu, A.Y.H., Junk, K.W. and Coon, M.J. (1969) *J. Biol. Chem.*, **244**, 3714–3721.
Majumdar, A., Wang, H., Morshauser, R.C. and Zuiderweg, E.R.P. (1993) *J. Biomol. NMR*, **3**, 387–397.
Muhandiram, D.R. and Kay, L.E. (1994) *J. Magn. Reson.*, **B103**, 203–216.
Narayanasami, R., Otvos, J.D., Kasper, C.B., Shen, A., Rajagopalan, J., McCabe, T.J., Okita, J.R., Hanahan, D.J. and Masters, B.S.S. (1992) *Biochemistry*, **31**, 4210–4218.
Pascal, S.M., Muhandiram, D.R., Yamazaki, T., Forman-Kay, J.D. and Kay, L.E. (1994) *J. Magn. Reson.*, **B103**, 197–201.
Peelen, S. and Vervoort, J. (1994) *Arch. Biochem. Biophys.*, **314**, 291–300.
Peelen, S., Wijmenga, S.S., Erbel, P.J.A., Robson, R.L., Eady, R.R. and Vervoort, J. (1996) *J. Biomol. NMR*, **7**, 315–330.
Phillips, A.H. and Langdon, R.G. (1962) *J. Biol. Chem.*, **237**, 2652–2660.
Piotto, M., Saudek, V. and Sklenář, V. (1992) *J. Biomol. NMR*, **2**, 661–665.
Porter, T.D. and Kasper, C.B. (1986) *Biochemistry*, **25**, 1682–1687.
Porter, T.D. (1991) *Trends Biochem. Sci.*, **16**, 154–158.
Rao, S.T., Shaffie, F., Yu, C., Satyshur, K.A., Stockman, B.J. and Sundaralingam, M. (1992) *Protein Sci.*, **1**, 1413–1427.
Romero, A., Caldeira, J., LeGall, J., Moura, I., Moura, J.J.G. and Romao, M.J. (1996) *Eur. J. Biochem.*, **239**, 190–196.
Sali, A. and Blundell, T.L. (1993) *J. Mol. Biol.*, **234**, 779–815.
Sevrioukova, I. and Peterson, J.A. (1995) *Biochimie*, **77**, 562–572.
Sevrioukova, I., Shaffer, C., Ballou, D.P. and Peterson, J.A. (1996) *Biochemistry*, **35**, 7058–7068.
Smith, G.C.M., Tew, D.G. and Wolf, C.R. (1994) *Proc. Natl. Acad. Sci. USA*, **91**, 8710–8714.
Stockman, B.J., Euvrard, A., Kloosterman, D.A., Scahill, T.A. and Swenson, R.P. (1993) *J. Biomol. NMR*, **3**, 133–149.
Strobel, H.W., Hodgson, A.V. and Shen, S. (1995) In *Cytochrome P450: Structure, Mechanism and Biochemistry*, 2nd ed. (Ed., Ortiz de Montellano, P.R.), Plenum, New York, NY, U.S.A., pp. 225–244.
Vuister, G.W., Clore, G.M., Gronenborn, A.M., Powers, R., Garrett, D.S., Tshudin, R. and Bax, A. (1993) *J. Magn. Reson.*, **B101**, 210–213.
Walton, M.I., Wolf, C.R. and Workman, P. (1992) *Biochem. Pharmacol.*, **44**, 251–259.
Watt, W., Tulinsky, A., Swenson, R.P. and Watenpaugh, K.D. (1991) *J. Mol. Biol.*, **218**, 195–208.
Williams, C.H. and Kamin, H. (1962) *J. Biol. Chem.*, **237**, 587–595.
Wishart, D.S. and Sykes, B.D. (1994) *J. Biomol. NMR*, **4**, 171–180.
Zhang, O., Kay, L.E., Oliver, J.P. and Forman-Kay, J.D. (1994) *J. Biomol. NMR*, **4**, 845–858.
Zhao, Q., Smith, G., Paine, M., Wolf, C.R., Tew, D., Modi, S., Lian, L.-Y., Primrose, W.U., Roberts, G.C.K. and Driessen, H. (1996) *J. Struct. Biol.*, **116**, 320–325.